

Spiral antiferromagnets beyond the spin-wave approximation: frustrated XY and Heisenberg models in the honeycomb lattice

Andrea Di Ciolo,¹ Juan Carrasquilla,^{2,3} Federico Becca,⁴ Marcos Rigol,³ and Victor Galitski¹

¹*Joint Quantum Institute and Department of Physics,
University of Maryland, College Park, 20742, USA*

²*Perimeter Institute for Theoretical Physics, Waterloo, Ontario, N2L 2Y5, Canada*

³*Department of Physics, The Pennsylvania State University, University Park, Pennsylvania 16802, USA*

⁴*Democritos National Simulation Center, Istituto Officina dei Materiali del CNR and
SISSA-International School for Advanced Studies, Via Bonomea 265, I-34136 Trieste, Italy*

We examine the stability of classical states with a generic incommensurate spiral order against quantum fluctuations. Specifically, we focus on the frustrated spin-1/2 XY and Heisenberg models on the honeycomb lattice with nearest-neighbor J_1 and next-nearest-neighbor J_2 antiferromagnetic couplings. Our variational approach is based on the Jastrow wave functions, which include quantum correlations on top of classical spin waves. We perform a systematic optimization of wave vectors and Jastrow pseudo-potentials within this class of variational states and find that quantum fluctuations favor collinear states over generic coplanar spirals. The Néel state with $\mathbf{Q} = (0, 0)$ extends its stability well beyond the classical value $J_2/J_1 = 1/6$. Most importantly, the collinear states with $\mathbf{Q} = (0, 2\pi/\sqrt{3})$ (and the two symmetry-related states) are found to be stable in a large regime with intermediate frustration, while at the classical level they are limited to the point $J_2/J_1 = 0.5$. For large frustration, the 120° state is stabilized for finite values of J_2/J_1 in both models.

I. INTRODUCTION

Magnetic frustration in spin systems is responsible for complex phase diagrams due to the competition between states that are very close in energy but exhibit fundamentally different properties [1]. Although exotic phases with no magnetic order (possibly having topological order and fractional excitations) represent the forefront of present research in the field, understanding complex magnetically ordered phases in quantum spin models remains of great interest as well. Indeed, at present spin liquids are found in only relatively small regions of frustrated spin models, such as the J_1 - J_2 model on the square lattice [2, 3] or the Heisenberg model on the kagome lattice [4, 5]. On the other hand, ordered phases are ubiquitous and represent important examples of correlated states [1].

The first step and simplest approximation in describing these phases is obtained by considering spins as classical variables, thus completely neglecting quantum fluctuations. This approximation is adequate when the spin S is large, e.g., for half-filled d or f shells in the presence of a large Hund coupling (mathematically speaking, this approximation becomes exact when $S = \infty$). In order to include quantum corrections, a systematic perturbative approach can be constructed by using the so-called Holstein-Primakoff transformation [6]. Here, the first-order terms at the $O(1/S)$ level already contain quantum correlations that correctly describe the low-energy spin-wave spectrum. In addition, within this scheme, it is possible to obtain rather accurate results for the renormalization of the magnetization due to quantum fluctuations. The $O(1/S)$ quantum corrections may also select the correct ground state when the classical ground state is highly degenerate, e.g., for the J_1 - J_2 model on the square lattice for $J_2/J_1 > 0.5$ [7]. Unfortunately, this technique becomes very cumbersome when considering higher cor-

rections beyond $O(1/S)$. Alternative approaches exist, e.g., a modified spin-wave theory [8], but they too involve complicated perturbative expansions. Therefore, identification of simple variational wave functions is useful to go beyond the spin-wave approximation and capture non-perturbative effects. Indeed, this approach has been widely used to study different spin models on frustrated lattices [9–13].

Among frustrated spin models, a particularly interesting example is the J_1 - J_2 Heisenberg model on the honeycomb lattice:

$$H_{\text{Heis}} = J_1 \sum_{\langle ij \rangle} \mathbf{S}_i \cdot \mathbf{S}_j + J_2 \sum_{\langle\langle ij \rangle\rangle} \mathbf{S}_i \cdot \mathbf{S}_j, \quad (1)$$

where the sums $\langle ij \rangle$ and $\langle\langle ij \rangle\rangle$ run over all the nearest-neighbor and next-nearest-neighbor bonds, respectively; $\mathbf{S}_i = (S_i^x, S_i^y, S_i^z)$ is the spin operator on site i . In the following, we consider $\mathbf{a} = (1, 0)$ and $\mathbf{b} = (-1/2, \sqrt{3}/2)$ as the two Bravais vectors defining the honeycomb lattice.

In recent years, a lot of effort has focused on understanding the phase diagram of this model, mainly in the case of antiferromagnetic Heisenberg interactions [14–23]. Interestingly, the J_1 - J_2 model on the honeycomb lattice has a non-trivial phase diagram even at the classical level, since for $J_2/J_1 > 1/6$ the ground state has an infinite degeneracy due to the fact that the wave vector \mathbf{Q} can vary on closed contours in the Brillouin zone; see below [24, 25]. The spin-1/2 quantum model has been the subject of recent works, and was shown to exhibit magnetically disordered regions for sufficiently large frustration, which presumably have plaquette and dimer orders [21–23].

A closely related model that also exhibits a rich phase diagram is the frustrated spin-1/2 XY model in the hon-

eycomb geometry:

$$H_{XY} = J_1 \sum_{\langle ij \rangle} (S_i^x S_j^x + S_i^y S_j^y) + J_2 \sum_{\langle\langle ij \rangle\rangle} (S_i^x S_j^x + S_i^y S_j^y). \quad (2)$$

By using the fact that $S_j^\pm = S_j^x \pm iS_j^y$, the spin-1/2 XY model is equivalent to “non-interacting” hardcore bosons with hopping amplitudes $J_1/2$ and $J_2/2$ at nearest- and next-nearest-neighbor sites, respectively [26, 27]. By using exact diagonalizations on small clusters, it was suggested that a disordered spin-liquid phase may appear in a narrow regime of intermediate frustration, in between magnetically ordered antiferromagnetic and collinear phases [26]. This scenario is consistent with variational calculations involving partonic wave functions [28]. However, recent density-matrix renormalization group calculations have instead pointed toward an unexpected ordered phase (with spin order along the z -axis, which is equivalent to a charge-density wave in the boson language) [29]. Both these scenarios are highly unusual and currently the nature of the ground state for $0.2 \lesssim J_2/J_1 \lesssim 0.3$ is not understood.

Both exact-diagonalization and density-matrix renormalization group studies are done in finite systems with highly constrained geometries. The complex quantum states that these methods select are in competition with other ordered states, including spirals that are often suggested by the classical analysis. The stabilization of these spirals may be highly frustrated in finite systems, which generates concerns about extrapolating finite-size results to the thermodynamic limit. Therefore, it is important to carry out a systematic study of these spiral states on large lattices and including quantum fluctuation around classical ground states. This is the focus of our work.

Our approach is based on introducing Jastrow wave functions that are particularly suitable to describe magnetically ordered states [9, 13]. These variational states are constructed by applying a long-range Jastrow factor, which enables us to account for quantum effects, to classical spin waves with a given wave vector \mathbf{Q} and relative phase η between the two spins in the unit cell (the detailed description is given in Sec. III). We show that the best Jastrow state may have a \mathbf{Q} vector different from the one that minimizes the classical energy. In general, collinear phases are highly favored over generic spiral ones. In particular, the Néel state with $\mathbf{Q} = (0, 0)$ remains stable up to $J_2/J_1 \simeq 0.3$ in the Heisenberg model and $J_2/J_1 \simeq 0.26$ for the XY model (to be compared with $J_2/J_1 = 1/6$ for the classical model). Moreover, a collinear state with $\mathbf{Q} = (0, 2\pi/\sqrt{3})$ (and the other two symmetry-related wave vectors) is remarkably stable in a wide region of the phase diagram, namely, $0.7 \lesssim J_2/J_1 \lesssim 1.4$ for the Heisenberg model and $0.26 \lesssim J_2/J_1 \lesssim 1$ for the XY model. While incommensurate spiral states are clearly defeated for small and intermediate values of J_2/J_1 , they may survive in a relatively small range of frustration, before the 120° state sets in.

The paper is organized as follows: In Sec. II, we provide a short summary of the classical results. In Sec. III, we

discuss the form of the variational states that are used. In Sec. IV, we show our numerical results, and, finally, in Sec. V, we draw our conclusions.

II. CLASSICAL RESULTS

Here, we briefly summarize the classical results [14, 24], which apply for both Heisenberg and XY models. Assuming coplanar order in the XY plane, the spins on the two sublattices are

$$\mathbf{S}_i = S \left[\cos(\mathbf{Q} \cdot \mathbf{R}_i), \sin(\mathbf{Q} \cdot \mathbf{R}_i), 0 \right] \quad (3)$$

when the site i belongs to the \mathcal{A} sublattice, and

$$\mathbf{S}_i = -S \left[\cos(\mathbf{Q} \cdot \mathbf{R}_i + \eta), \sin(\mathbf{Q} \cdot \mathbf{R}_i + \eta), 0 \right] \quad (4)$$

when the site i belongs to the \mathcal{B} sublattice. Here, \mathbf{R}_i denotes the coordinates of the site i in the triangular Bravais lattice, the two sites in the unit cell having the same \mathbf{R}_i . \mathbf{Q} is the spiral wave vector, and $\eta + \pi$ (notice the definition with the minus sign for spins on the \mathcal{B} sublattice) defines the angle between the two spins on different sublattices. Within this notation, the Néel antiferromagnet is described by $\mathbf{Q} = \mathbf{\Gamma} = (0, 0)$ and $\eta = 0$ while the state with 120° order has $\mathbf{Q} = \mathbf{K} = (4\pi/3, 0)$ or $\mathbf{K}' = (2\pi/3, 2\pi/\sqrt{3})$ and an arbitrary phase shift (the two sublattices being totally decoupled). The classical energy per spin for a generic coplanar spin wave can be written as

$$E_{\text{cl}} = -\frac{J_1 S^2}{2} \left[\cos \eta + \cos(\eta - Q_b) + \cos(\eta - Q_a - Q_b) \right] + J_2 S^2 \left[\cos Q_a + \cos Q_b + \cos(Q_a + Q_b) \right], \quad (5)$$

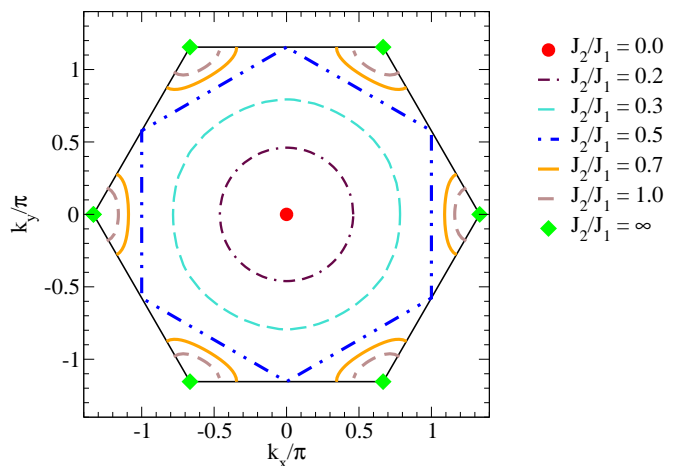


FIG. 1. (Color online) The manifold of classically degenerate spiral wave vectors for a few values of J_2/J_1 . For $J_2/J_1 < 1/6$, the lowest-energy state has $\mathbf{Q}^* = (0, 0)$, while for $J_2/J_1 > 1/6$ the ground state is degenerate: the \mathbf{Q}^* wave vectors form closed contours around the $\mathbf{\Gamma}$ point for $1/6 < J_2/J_1 < 1/2$ and around the \mathbf{K} (or \mathbf{K}') point for $J_2/J_1 > 1/2$. For $J_2/J_1 \rightarrow \infty$, $\mathbf{Q}^* = \mathbf{K}$ or \mathbf{K}' .

where $Q_a = \mathbf{Q} \cdot \mathbf{a} = Q_x$ and $Q_b = \mathbf{Q} \cdot \mathbf{b} = -Q_x/2 + \sqrt{3}Q_y/2$. By minimizing the classical energy with respect to Q_a , Q_b , and η , one finds two regimes: for $J_2/J_1 < 1/6$, the lowest-energy state has $\mathbf{Q}^* = (0, 0)$ and $\eta^* = 0$, while for $J_2/J_1 > 1/6$ it has a finite \mathbf{Q}^* satisfying the relation

$$\cos Q_a^* + \cos Q_b^* + \cos(Q_a^* + Q_b^*) = \frac{1}{2} \left[\left(\frac{J_1}{2J_2} \right)^2 - 3 \right], \quad (6)$$

while η^* is completely defined by

$$\sin \eta^* = \frac{2J_2}{J_1} [\sin Q_b^* + \sin(Q_a^* + Q_b^*)], \quad (7)$$

$$\cos \eta^* = \frac{2J_2}{J_1} [1 + \cos Q_b^* + \cos(Q_a^* + Q_b^*)]. \quad (8)$$

Given Eq. (6), there are infinite spiral wave vectors that minimize the energy at any given value of $J_2/J_1 > 1/6$.

In Fig. 1, we report the classically degenerate solutions for a few values of J_2/J_1 : they form closed contours around Γ for $1/6 < J_2/J_1 < 1/2$ (spirals I) and around \mathbf{K} or \mathbf{K}' for $J_2/J_1 > 1/2$ (spirals II). For $J_2/J_1 = 1/2$, the closed contour has a hexagonal shape and, among all possible spirals, there are three particularly simple collinear states, in which all nearest-neighbor bonds along one direction are ferromagnetic, while the other two are antiferromagnetic. One of these states has $\mathbf{Q} = \mathbf{M} = (0, 2\pi/\sqrt{3})$ and $\eta = \pi$. These collinear states are stabilized in a wide region of the phase diagram when quantum fluctuations are considered. The 120° state is recovered only when $J_2/J_1 \rightarrow \infty$, i.e., when the two sublattices are totally decoupled. Real-space spin configurations for some representative states described above are depicted in Fig. 2.

Finally, we mention the fact that the $O(1/S)$ quantum corrections lift the huge classical degeneracy for $J_2/J_1 > 1/6$, selecting wave vectors along Γ - \mathbf{M} (and symmetry-related ones) for $J_2/J_1 < 1/2$ and along the border zone for $J_2/J_1 > 1/2$ [14]. In the following, we will analyze the extent to which the $O(1/S)$ scenario is preserved for $S = 1/2$ models.

III. VARIATIONAL WAVE FUNCTIONS

The variational states containing quantum fluctuations are defined by:

$$|\Psi\rangle = \mathcal{J}_z \mathcal{P}_{S_{\text{tot}}^z=0} |\text{SW}\rangle. \quad (9)$$

Here, $|\text{SW}\rangle$ is a spin-wave state, described by a wave vector \mathbf{Q} and a phase shift η :

$$\begin{aligned} |\text{SW}\rangle &= \prod_i \left(|\downarrow\rangle_i + e^{i(\mathbf{Q} \cdot \mathbf{R}_i + \eta_i)} |\uparrow\rangle_i \right) \\ &= \prod_i e^{i(\mathbf{Q} \cdot \mathbf{R}_i + \eta_i)(S_i^z + 1/2)} (|\downarrow\rangle_i + |\uparrow\rangle_i), \end{aligned} \quad (10)$$

where $\eta_i = 0$ if i belongs to sublattice \mathcal{A} and $\eta_i = \eta + \pi$ if it belongs to sublattice \mathcal{B} . $|\text{SW}\rangle$ is equivalent to a classical state where each spin points in a given direction in

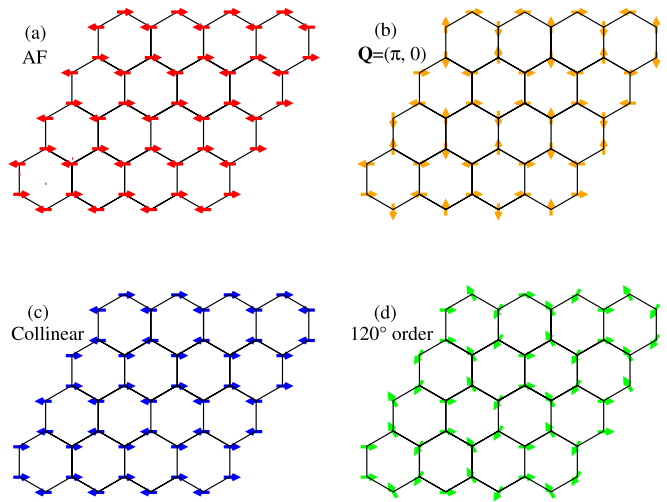


FIG. 2. (Color online) Real-space illustration of some of the ordered states considered in this work. (a) Néel antiferromagnet, for which $\mathbf{Q} = \Gamma = (0, 0)$ and $\eta = 0$. (b) $(\pi, 0)$ -spiral, for which $\mathbf{Q} = (\pi, 0)$ and $\eta = 0$. (c) Collinear state, for which $\mathbf{Q} = \mathbf{M} = (0, 2\pi/\sqrt{3})$ and $\eta = \pi$. (d) 120° ordered phase, for $\mathbf{Q} = \mathbf{K}$ or \mathbf{K}' and η arbitrary.

the XY plane. $\mathcal{P}_{S_{\text{tot}}^z=0}$ is the projector onto the subspace with $S^z = 0$. When projected into this subspace, $|\text{SW}\rangle$ is translationally invariant, since for example:

$$\mathcal{T}_{\mathbf{a}} |\text{SW}\rangle = e^{i\mathbf{Q} \cdot \mathbf{a}(S_{\text{tot}}^z + N)} |\text{SW}\rangle, \quad (11)$$

where $\mathcal{T}_{\mathbf{a}}$ is the translational operator of one lattice site along \mathbf{a} and N is the number of sites of the Bravais lattice, $\mathbf{Q} \cdot \mathbf{a}N = 0 \pmod{2\pi}$.

Quantum fluctuations are included through the long-range Jastrow factor

$$\mathcal{J}_z = \exp \left(\frac{1}{2} \sum_{ij} v_{ij} S_i^z S_j^z \right), \quad (12)$$

where, in a translationally invariant system, the pseudopotential v_{ij} depends upon the vector $\mathbf{R}_i - \mathbf{R}_j$. All the independent parameters (i.e., the v_{ij} 's as well as \mathbf{Q} and η) are optimized via Monte Carlo simulations in order to minimize the variational energy [30, 31].

Quantum fluctuations in the spin-1/2 case are expected to be strong enough to substantially change the classical scenario. We would like to emphasize that we consider only two-body correlations; higher-order terms have been used to improve both the signs and the amplitudes of variational states in frustrated lattices [11]. Indeed, while our wave function has the correct signs for the unfrustrated case with $J_2 = 0$ (where a Marshall sign rule holds), in general it does not reproduce the correct (and unknown) sign structure. We would like also to remark that the variational state explicitly breaks the spin $SU(2)$ symmetry of the Heisenberg model. This is apparent from the fact that the order parameter is in the

XY plane, and the Jastrow factor contains only the z component of the spin operator.

Since quantum effects may favor states with a different ordering vector than the one selected by the classical model, we compute the energy by optimizing the Jastrow parameters for all non-equivalent spin waves allowed by the particular lattice size and study an extensive range of values of η in order to determine the state with the lowest possible energy. It should be emphasized that not all possible \mathbf{Q} vectors are accessible on finite clusters. This fact is particularly relevant when considering spirals, which may be frustrated on a given finite lattice; nonetheless, it is still possible to follow the evolution of the wave vector as a function of the frustrating ratio J_2/J_1 and to detect the stability of collinear phases.

Finally, it is important to note that classical states with generic \mathbf{Q} do not in general possess the underlying rotational invariance of the lattice, i.e., pairs of spins along different spatial orientations and the same geometric distance apart might be correlated in different ways. When attempting to build correlations on top of such states, those differences are naturally accounted for in our trial states by considering a Jastrow factor with parameters v_{ij} that allow for the breaking of rotational invariance of the lattice.

IV. RESULTS

In what follows, we explore the extent to which the classical scenario is modified by quantum fluctuations in the spin-1/2 XY and Heisenberg models. We determine the spin-ordered variational states for $0 \leq J_2/J_1 \leq 5$ by performing extensive Monte Carlo simulations for various $(L \times L \times 2)$ -site clusters (L being the number of unit cells along \mathbf{a} and \mathbf{b}), with $L = 4, 6, 8, 10, 12, 14, 16$, and 18 ($L = 20$ was simulated for a few selected values of J_2/J_1). We also report the energies extrapolated in the thermodynamic limit. The comparison with exact results on a small $L = 4$ cluster for both the XY and the Heisenberg models is presented in the Appendix.

A. Quantum XY model

To identify the presence of possible spirals, one needs to carefully investigate large cluster sizes. However, even for rather large cluster sizes, only a discrete number of wave vectors are available (i.e., $\mathbf{q} = 2\pi/L[n, (2m - n)/\sqrt{3}]$, n and m being integers) and incommensurate spirals cannot be captured. Nonetheless, it is possible to reach a quite detailed understanding of the evolution of the wave vector describing ordered states.

In Fig. 3, we report the wave vectors \mathbf{Q} that give the lowest energies of the Jastrow states [Eq. (9)] for different values of J_2/J_1 . The corresponding energies are reported in Fig. 4 for $0 \leq J_2/J_1 \leq 1$ (a) and $1 \leq J_2/J_1 \leq 5$ (b). These results are obtained in clusters with $18 \times 18 \times 2$

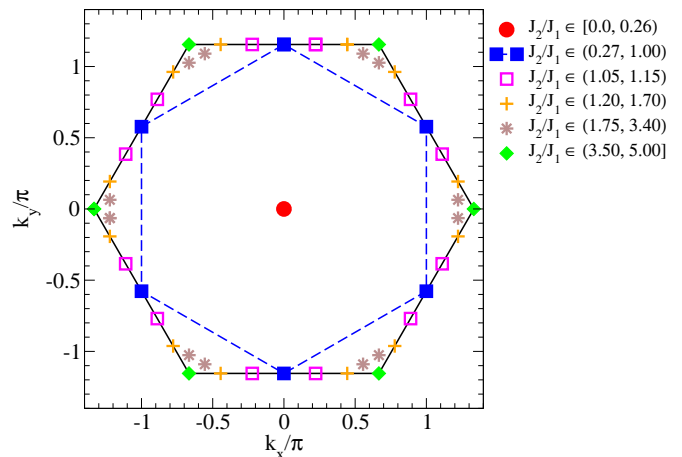


FIG. 3. (Color online) The locus of wave vectors for different values of J_2/J_1 giving the minimal energy of the Jastrow variational wave functions. The results are shown for the XY model with $L = 18$ (i.e., 648 sites).

sites and the typical statistical errors for our energies are of the order of $10^{-6}J_1$, i.e., the size of the data points greatly exceeds our error bars.

These results show three remarkable effects of quantum fluctuations: (i) a prolongation of the stability of the Néel antiferromagnetic phase with $\mathbf{Q} = (0, 0)$ up to $J_2/J_1 \simeq 0.26$, (ii) the extension of the stability of the collinear state from a point at $J_2/J_1 = 1/2$ to an entire region $0.26 \lesssim J_2/J_1 \lesssim 1$, and (iii) the extension of the stability of the 120° state from a point at $J_1/J_2 = 0$ to an entire region with $J_2/J_1 \gtrsim 3.5$. In particular, we find that spirals I disappear from the phase diagram and only spirals II occur in the presence of quantum fluctuations, between the collinear and the 120° states. Moreover, quan-

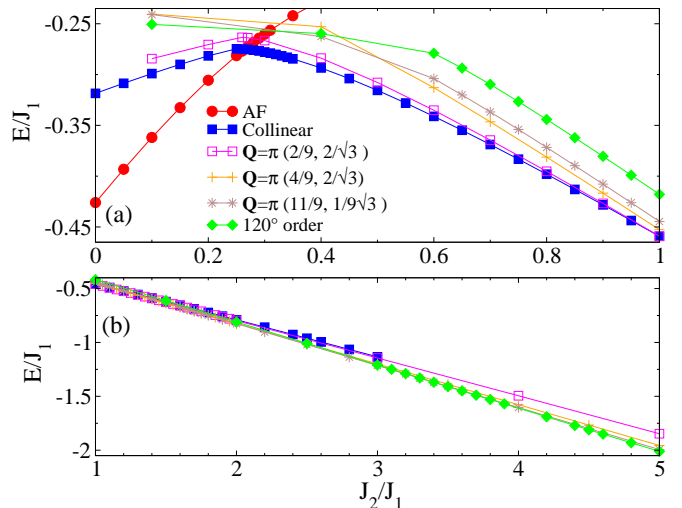


FIG. 4. (Color online) Variational energies for the XY model for $0 \leq J_2/J_1 \leq 1$ (a) and $1 \leq J_2/J_1 \leq 5$ (b) as a function of J_2/J_1 for $L = 18$. Statistical errors are smaller than the symbols and solid lines are provided as a guide to the eye.

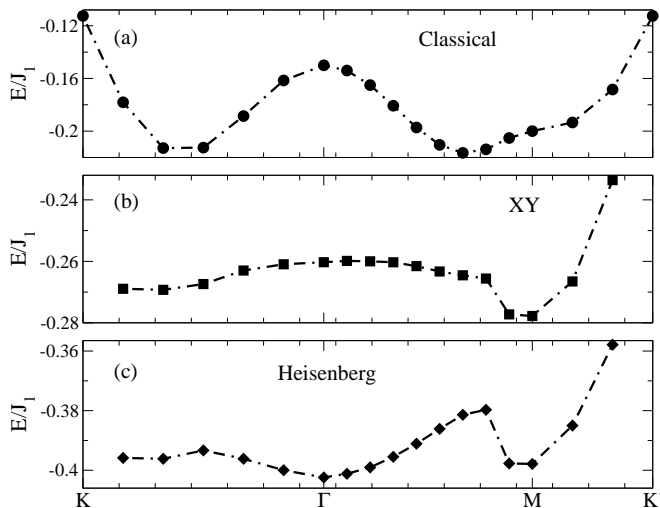


FIG. 5. Energy versus wave vector for classical (a), XY (b), and Heisenberg (c) models for $J_2/J_1 = 0.3$ and $L = 18$.

tum fluctuations determine an order-by-disorder lifting of the huge classical degeneracy, the wave vector of spiral phases being always along $\mathbf{M}\text{-}\mathbf{K}'$ (finite-size effects may favor wave vectors that are close to but not exactly along the border zone). Unfortunately, even on the $L = 18$ cluster there are only two \mathbf{q} points between \mathbf{M} and \mathbf{K}' and, therefore, it is extremely difficult to follow the evolution of the wave vector for $J_2/J_1 \gtrsim 1$.

We should add that, as seen in Fig. 4, the difference in energy between the competing spirals and the collinear and 120° states is very small. This suggests the possibility that spirals may disappear altogether in the thermodynamic limit, i.e., that quantum corrections favor spirals with relatively short periods such as the collinear and 120° states. Another possibility is that, as one increases the system size, new spirals will appear between the collinear and 120° states, pushing the stability region of the latter state to higher values of J_2/J_1 .

In Fig. 5(b), we report the energy of the XY model as a function of the wave vector along the highly symmetric lines in the Brillouin zone for $J_2/J_1 = 0.3$; the classical results are reported in Fig. 5(a) for comparison. Figure 5(b) makes apparent that quantum fluctuations dramatically reduce the dependence of the energy on the wave vectors along these lines. Furthermore, and more importantly, the minimum in the energy is shifted from spirals I (here along $\Gamma\text{-}\mathbf{M}$) to the collinear state with $\mathbf{Q} = \mathbf{M}$.

Having explored the various spin configurations for several cluster sizes, we have also done a finite-size scaling analysis of the energy for $0 \leq J_2/J_1 \leq 1$, where the Néel and collinear states are found to be the lowest energy states in all sizes considered here. The thermodynamic value for the energy per site can be obtained from [32–34]

$$E = E_\infty - \frac{C}{L^3} + \frac{D}{L^4}, \quad (13)$$

J_2/J_1	Spin-wave state	E_∞	C	Classical E
0.0	Néel	-0.425946(1)	0.195(1)	-0.3750000
0.1	Néel	-0.361879(1)	0.142(1)	-0.3000000
0.2	Néel	-0.305560(2)	0.092(2)	-0.2312500
0.3	Collinear	-0.277761(2)	0.115(3)	-0.2166667
0.4	Collinear	-0.293475(1)	0.123(2)	-0.2281250
0.5	Collinear	-0.315539(1)	0.138(2)	-0.2500000
0.6	Collinear	-0.341104(2)	0.139(2)	-0.2770833
0.7	Collinear	-0.368848(2)	0.114(3)	-0.3071428
0.8	Collinear	-0.398038(2)	0.075(3)	-0.3390625
0.9	Collinear	-0.428247(3)	0.04(1)	-0.3722222
1.0	Collinear	-0.459214(3)	0.00(1)	-0.4062500

TABLE I. Extrapolated energies of the variational Jastrow state in the thermodynamic limit in the spin-1/2 XY model for $0 < J_2/J_1 < 1$. We also report the value of C in Eq. (13) and the classical prediction for the energy.

where E_∞ is the energy in the thermodynamic limit; the fitting parameters $C = \beta c_{\text{sw}}^2$ and $D = \alpha c_{\text{sw}}^2 / \rho_s$ provide information about the spin-wave velocity c_{sw} and the spin stiffness ρ_s (α and β are parameters that depend upon the details of the lattice).

Typical examples of the application of this extrapolation procedure are shown in Fig. 6. For the cluster sizes utilized to determine E_∞ , Eq. (13) provides an excellent description of the scaling of the data. The nearly linear behavior of the fits shows that the contribution of the leading L^{-3} correction to the thermodynamic limit result is dominant for the system sizes considered.

The extrapolated results for the energy in the thermodynamic limit, as well as the classical predictions, are

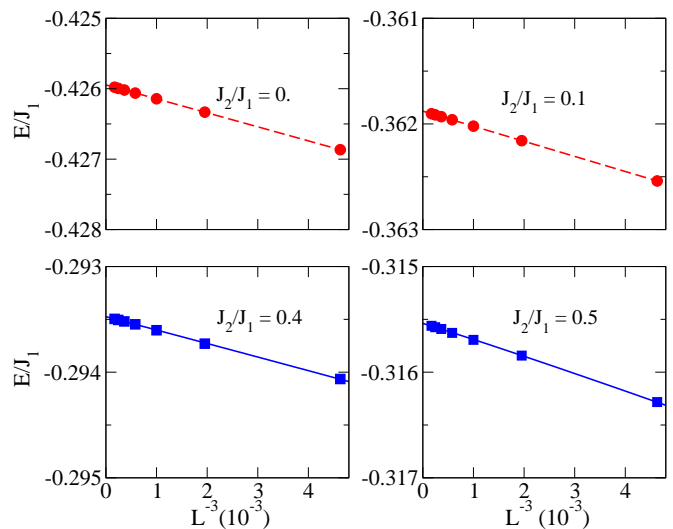


FIG. 6. (Color on-line) Finite-size scaling of the energy of the spin-1/2 XY model for different values of J_2/J_1 in the Néel and collinear phases. Lines depict the results of fits according to Eq. (13). Red circles (blue squares) indicate the Néel (collinear) phase.

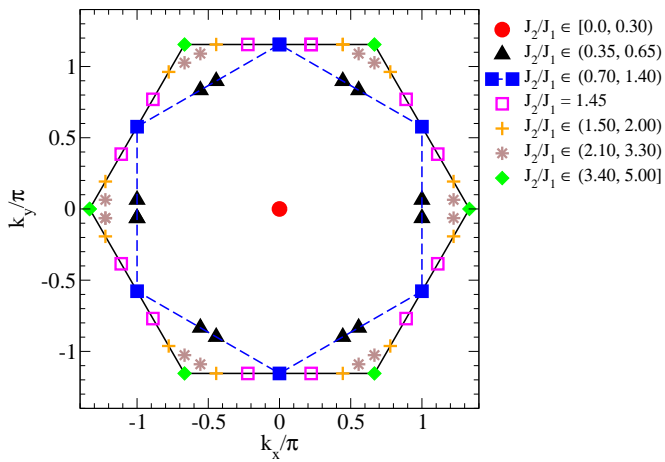


FIG. 7. (Color online) The same as Fig. 3, but for the Heisenberg model.

reported in Table I. A comparison between the two makes apparent that the addition of quantum fluctuations dramatically reduces the energy of the ordered states. The values obtained for C [see Eq. (13)] are also reported in Table I. If one assumes that β changes moderately with frustration, the evolution of C resembles the behavior of the spin-wave velocity c_{sw} . We find that C has a local minimum around the transition between the Néel and the collinear phases. Most importantly, our results indicate that the spin-wave velocity remains finite at the transition. In addition, C is seen to decrease and vanish as one approaches the transition between the collinear state and the spirals, which occurs for $J_2/J_1 \simeq 1$.

B. Quantum Heisenberg model

We now study what happens to the ordered phases in the Heisenberg model and show that, in this case also, quantum fluctuations strongly modify the classical picture favoring collinear states.

In Fig. 7, we report the evolution of the wave vector upon increasing frustration on a $(18 \times 18 \times 2)$ -site cluster. The results can be seen to be quite similar to those for the XY model (see Fig. 3), with an important difference that we highlight in what follows. The corresponding energies as a function of J_2/J_1 are reported in Fig. 8. The results for this large cluster provide strong indications of the trends in the thermodynamic limit. First of all, the stability of the Néel state persists up to $J_2/J_1 \simeq 0.3$, which is even larger than what was found in the XY model. Starting at that point, the best energy is given by the spiral with $\mathbf{Q} = (\pi, 0)$: in the $18 \times 18 \times 2$ cluster this wave vector is not present and the best energy is found for $\mathbf{Q} = (\pi, \pi/9\sqrt{3})$, which is the closest point to $\mathbf{Q} = (\pi, 0)$. For smaller clusters having $(\pi, 0)$, we have checked that the spiral with $\mathbf{Q} = (\pi, 0)$ is indeed the ordered state with the lowest energy. This spiral state is stable up to $J_2/J_1 \simeq 0.7$. Therefore, the stability region

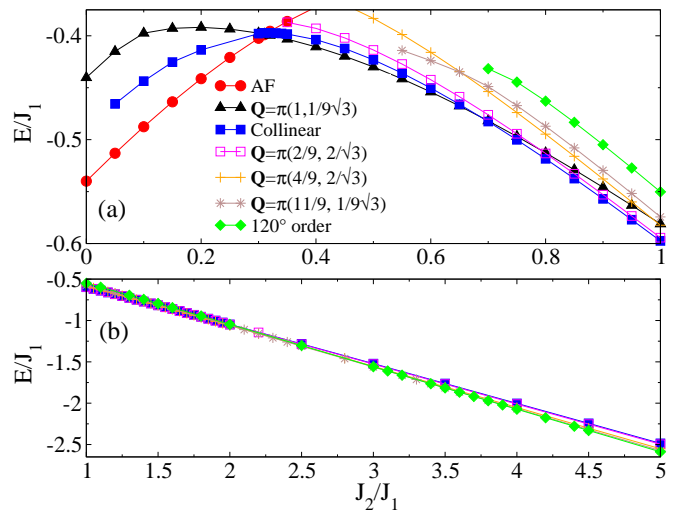


FIG. 8. (Color online) The same as Fig. 4, but for the Heisenberg model.

of this spiral phase is greatly enhanced with respect to the classical case, where the $(\pi, 0)$ spiral is stable only for $J_2/J_1 = 0.5$. For $J_2/J_1 \gtrsim 0.7$, on the other hand, we find that the collinear state with $\mathbf{Q} = \mathbf{M}$ becomes lower in energy. On further increasing frustration, i.e., for $J_2/J_1 \simeq 1.4$, other spirals (with wave vector along $\mathbf{M}-\mathbf{K}'$, similarly to the XY model) become lower in energy. Finally, for $J_2/J_1 \gtrsim 3.4$ the 120° state is found to be the best variational state.

As in the XY model, quantum fluctuations lift the degeneracy between the states with $\mathbf{Q} = (\pi, 0)$ and $\mathbf{Q} = (0, 2\pi/\sqrt{3})$. For example, on the $18 \times 18 \times 2$ cluster, the energies of the states with $\mathbf{Q} = (\pi, \pi/9\sqrt{3})$ and $\mathbf{Q} = (0, 2\pi/\sqrt{3})$ are $E = -0.430003(5)$ and $E = -0.423142(5)$, respectively, for $J_2/J_1 = 0.5$; while they are $E = -0.51265(1)$ and $E = -0.51849(1)$, respectively, for $J_2/J_1 = 0.8$. In Fig. 5(c), we report the results for the energy as a function of the wave vector for $J_2/J_1 = 0.3$ and $L = 18$. In this case, we can see the appreciable differences between the XY and Heisenberg models: in the former, the energy minimum is already at $\mathbf{Q} = \mathbf{M}$, while, in the latter, the energy minimum is still at $\mathbf{Q} = \mathbf{\Gamma}$, and local minima can be seen around $(\pi, 0)$ and $(0, 2\pi/\sqrt{3})$.

By comparing the results for the XY (see Fig. 4) and Heisenberg (see Fig. 8) models one can see that the main qualitative difference between them is the existence of a $(\pi, 0)$ spiral as the lowest energy state in the latter. Hence, while quantum fluctuations lift the degeneracy between the $(\pi, 0)$ spiral and the collinear state in both models, only in the Heisenberg model do these spirals appear as the ground state in our variational approach based upon Jastrow wave functions.

In Fig. 9, we show typical examples of the extrapolations done for the Heisenberg model in order to obtain the energy in the thermodynamic limit, where we have used the scaling in Eq. (13). As for the XY model (see Fig. 6), we have found that Eq. (13) provides an excel-

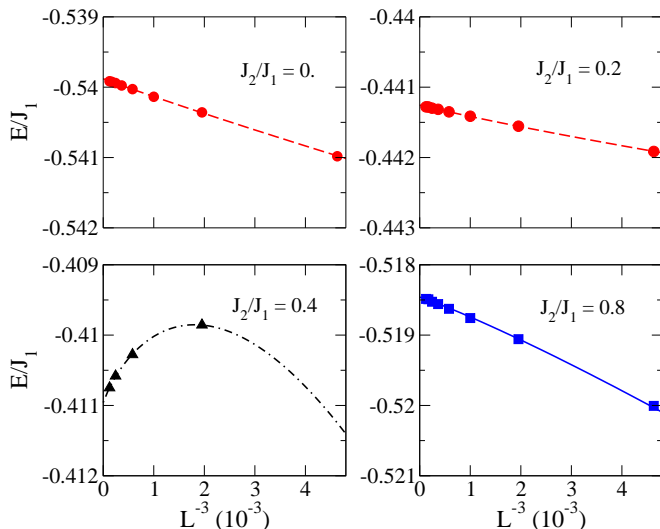


FIG. 9. (Color online) The same as Fig. 6 but for the Heisenberg model. Red circles (blue squares) indicate the Néel (collinear) phase. The black triangles indicate the $(\pi, 0)$ spiral.

lent description of the data for the Néel and collinear states. The nearly linear behavior of the fits makes apparent that the contribution of the leading L^{-3} correction to the thermodynamic result is dominant for the system sizes considered. In contrast, the finite-size trend for the $(\pi, 0)$ spiral shows an anomalous behavior, with a positive slope (i.e., a negative coefficient C). Moreover, in this case, a substantial contribution from the sub-leading corrections L^{-4} is present, i.e., our results for this state (which include the cluster with $L = 20$) suffer from strong finite-size effects. Hence, larger clusters and/or Jastrow factors with higher-order correlations are needed to clarify the fate of the $(\pi, 0)$ spiral in the thermodynamic limit.

Results for the extrapolated energies and corresponding orderings for the Heisenberg model in the thermodynamic limit are shown in Table II, where they can be compared to the classical predictions. As for the XY case, one can see that the addition of quantum fluctuations reduces the energy dramatically. In Table II, we also report the values of the fitting parameter C whenever it is positive. As discussed for the XY model, one can obtain information on the behavior of the spin-wave velocity c_{sw} from the coefficient C of the fitting procedure of Eq. (13). Here, C decreases upon increasing frustration but does not vanish at the transition from the antiferromagnetic state to the $(\pi, 0)$ -spiral. This behavior is similar to that observed in the XY model for the transition between the antiferromagnetic state and the collinear one.

J_2/J_1	Spin-wave state	E_∞	C	Classical E
0.0	Néel	-0.539880(2)	0.280(3)	-0.3750000
0.1	Néel	-0.487544(2)	0.230(3)	-0.3000000
0.2	Néel	-0.441254(2)	0.191(4)	-0.2312500
0.3	Néel	-0.402398(3)	0.127(4)	-0.2166667
0.4	$(\pi, 0)$ spiral	-0.410958(5)		-0.2281250
0.5	$(\pi, 0)$ spiral	-0.43051(1)		-0.2500000
0.6	$(\pi, 0)$ spiral	-0.45476(1)		-0.2770833
0.7	$(\pi, 0)$ spiral	-0.48261(1)		-0.3071428
0.8	Collinear	-0.518460(3)	0.198(6)	-0.3390625
0.9	Collinear	-0.556993(4)	0.153(8)	-0.3722222
1.0	Collinear	-0.597471(4)	0.084(9)	-0.4062500

TABLE II. Extrapolated energies of the variational Jastrow state in the thermodynamic limit in the spin-1/2 Heisenberg model for $0 < J_2/J_1 < 1$. We also report the value of C in Eq. (13), and the classical prediction for the energy.

V. CONCLUSIONS

We have explored the stability of classically ordered states within the phase diagram of the spin-1/2 XY and Heisenberg models on the honeycomb lattice, using long-range Jastrow wave functions and Monte Carlo simulations.

For the XY model, in the context of our variational calculations, we find that quantum fluctuations extend the stability of the antiferromagnetic state up to $J_2/J_1 \simeq 0.26$ (to be compared to $J_2/J_1 = 1/6$ in the classical case), of the collinear state for $0.26 \lesssim J_2/J_1 \lesssim 1$ (to be compared to $J_2/J_1 = 0.5$ in the classical case), and of the 120° phase for $J_2/J_1 \gtrsim 3.5$ (to be compared to $J_2/J_1 = \infty$ in the classical case). Quantum fluctuations are found to suppress spirals I, while spirals II still occur for $1 \lesssim J_2/J_1 \lesssim 3.5$, in between the collinear and 120° states. Since the difference in energy between spirals II and the collinear or 120° states is very small in the region where the former are the lowest-energy states in the finite clusters studied, an open question is whether those spirals remain stable in the thermodynamic limit, or whether they disappear and a direct transition occurs between collinear and 120° states.

A comparison between the results of our variational calculations for spirals in the spin-1/2 XY model to those of exact diagonalization (see the Appendix), partonic wave function studies [28], and density-matrix renormalization group calculations [29] makes apparent that in-plane magnetically ordered states are not expected to appear as ground states in the maximally frustrated region $0.2 \lesssim J_2/J_1 \lesssim 0.36$. On the contrary, magnetically ordered states described by Eq. (9) are expected to correctly describe the ground-state properties for both $J_2/J_1 \lesssim 0.2$ and probably $J_2/J_1 \gtrsim 0.36$ (for the latter case, more work is needed to understand the precise value of J_2 at which magnetic long-range order occurs).

For the Heisenberg model, we find that quantum fluc-

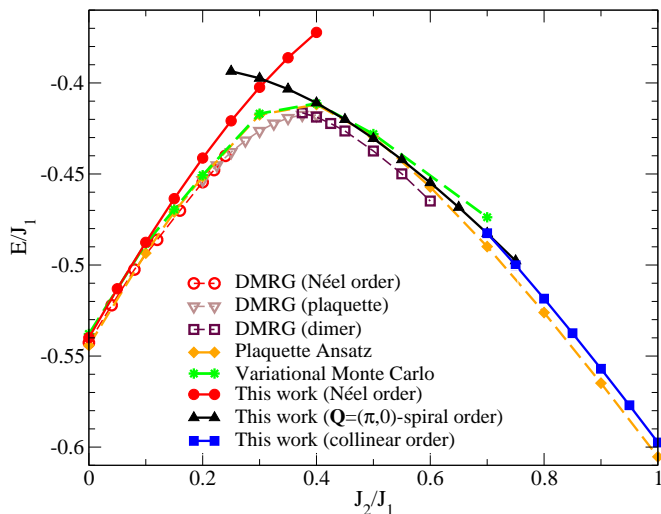


FIG. 10. (Color online) Comparison between our variational approach for magnetically ordered states and other numerical approaches that have been considered recently.

tuations extend the stability of the antiferromagnetic state up to $J_2/J_1 \simeq 0.3$ (to be compared to $J_2/J_1 = 1/6$ in the classical case), of the $(\pi, 0)$ spiral state for $0.3 \lesssim J_2/J_1 \lesssim 0.7$ (to be compared to $J_2/J_1 = 0.5$ in the classical case), of the collinear state for $0.7 \lesssim J_2/J_1 \lesssim 1.4$ (to be compared to $J_2/J_1 = 0.5$ in the classical case), and of the 120° phase for $J_2/J_1 \gtrsim 3.4$ (to be compared to $J_2/J_1 = \infty$ in the classical case). Spirals II appear for $1.4 \lesssim J_2/J_1 \lesssim 3.4$, between the collinear and 120° states. As in the XY case, since the difference in energy between spirals II and the collinear and 120° states is very small, their stability in the thermodynamic limit remains uncertain.

We note that, for our finite-size calculations of the spin-1/2 XY and Heisenberg models, quantum fluctuations lift the macroscopic classical degeneracy of spirals II favoring wave vectors along the border zone $\mathbf{M}\text{-}\mathbf{K}'$, in agreement with $O(1/S)$ spin-wave calculations [14]. In addition, they lift the degeneracy between the $(\pi, 0)$ spiral state and the collinear state. As a result, the former state disappears from the phase diagram of the XY model while its stability is enhanced in the Heisenberg one. However, we found that our results for the energy of the $(\pi, 0)$ -spiral state in the Heisenberg model exhibit strong finite-size effects, which suggests that they need to be reconsidered with calculations on larger clusters and/or including Jastrow factors with higher-order correlations.

Finally, we would like to briefly discuss the relation of our variational calculations of magnetically ordered phases with previous numerical calculations on the spin-1/2 Heisenberg model. In Fig. 10, we report the energy of our best states together with recent density-matrix renormalization group (DMRG) calculations [21], variational approaches based upon Jastrow and projected fermionic states [15], or plaquette *Ansätze* [20]. (A comparison

with exact diagonalization results for a 32-site cluster is presented in the Appendix). In general, ordered states provide accurate approximations for the exact ground state for small and large values of J_2/J_1 . Especially for $J_2/J_1 \lesssim 0.2$, our energies are competitive with the DMRG ones, indicating that the Néel ordered phase occurs in that regime. The DMRG result that the Néel phase is obtained beyond its classical stability region is fully compatible with our present results, showing that (in contrast to other results for frustrated lattices such as, for example, the J_1 - J_2 model on the square lattice) quantum fluctuations can reinforce collinear magnetic order.

On the contrary, our spin-wave states have a rather poor accuracy in the highly frustrated regime $0.2 \lesssim J_2/J_1 \lesssim 0.4$, where magnetically disordered phases with plaquette and dimer order should occur [21–23]. The $(\pi, 0)$ spiral state may disappear altogether, being replaced by disordered plaquette and dimer phases [21–23]. For larger values of J_2/J_1 , our ordered states become again competitive with other those from methods, indicating that magnetically ordered phases are present in that part of the phase diagram. In particular, the collinear phase with $\mathbf{Q} = (0, 2\pi/\sqrt{3})$ (and related ones) may be relevant for $J_2/J_1 \gtrsim 0.8$, where DMRG results [21] showed clear evidence of a rotational-symmetry breaking and possibly a vanishing spin gap.

VI. ACKNOWLEDGMENTS

This work was supported by the National Science Foundation under Grant No. OCI-0904597 (A.D.C. and M.R.), the Office of Naval Research (J.C. and M.R.), PRIN 2010-11 (F.B.), and the U.S. ARO (V.G.). J.C. acknowledges support from the John Templeton Foundation. Research at Perimeter Institute is supported by the Government of Canada through Industry Canada and by the Province of Ontario through the Ministry of Research & Innovation. We thank A. Parola for providing us with the exact results on the $4 \times 4 \times 2$ cluster shown in the Appendix; R. Ganesh for his DMRG results shown in Fig. 10; and C. N. Varney, K. Sun, and S. Nishimoto for stimulating discussions.

Appendix A: Comparison with exact results on a small cluster

In order to test the accuracy of our spin wave states, here we present a direct comparison between variational and exact energies on a small $(4 \times 4 \times 2)$ -site cluster for $0 \leq J_2/J_1 \leq 1$. The results for the energy are reported in Tables III and IV for the XY and Heisenberg models, respectively. In such a cluster, only a few spirals can be accommodated (there are only four independent momenta available). We mention that the exact ground state is always in the $\mathbf{Q} = (0, 0)$ subspace, for both the

J_2/J_1	Spin-wave state	E_{Jastrow}	E_{exact}	Accuracy
0.0	Néel	-0.429079(1)	-0.4294059	0.001
0.1	Néel	-0.364117(2)	-0.3654374	0.004
0.2	Néel	-0.306949(4)	-0.3149448	0.025
0.3	Collinear	-0.279516(4)	-0.2952758	0.053
0.4	Collinear	-0.295509(3)	-0.3016051	0.020
0.5	Collinear	-0.318238(3)	-0.3237236	0.017
0.6	Collinear	-0.344366(3)	-0.3502100	0.017
0.7	Collinear	-0.372495(4)	-0.3789541	0.017
0.8	Collinear	-0.401916(4)	-0.4090846	0.017
0.9	Collinear	-0.432229(4)	-0.4401615	0.018
1.0	Collinear	-0.463183(5)	-0.4719334	0.019

TABLE III. Comparison between the exact ground-state energies and the energies of the best Jastrow wave function on the $4 \times 4 \times 2$ cluster for the XY model.

XY and the Heisenberg models.

On the XY model, the agreement between the variational and the exact ground-state energies is excellent for the unfrustrated case (where it is about 0.1%). Then the accuracy deteriorates on increasing J_2/J_1 . The worst results are obtained in the highly frustrated regime $0.2 \leq J_2/J_1 \leq 0.4$, where a magnetically disordered phase is expected to occur in the thermodynamic limit. Then the accuracy is remarkably good also for $J_2/J_1 \gtrsim 0.4$, even though the variational state has a finite wave vector. On

J_2/J_1	Spin-wave state	E_{Jastrow}	E_{exact}	Accuracy
0.0	Néel	-0.54528(1)	-0.5516867	0.012
0.1	Néel	-0.49168(1)	-0.4998728	0.016
0.2	Néel	-0.44428(1)	-0.4567175	0.027
0.3	Collinear	-0.40600(1)	-0.4275835	0.050
0.4	$(\pi, 0)$ spiral	-0.41217(1)	-0.4203210	0.019
0.5	$(\pi, 0)$ spiral	-0.43401(1)	-0.4424316	0.019
0.6	$(\pi, 0)$ spiral	-0.46160(1)	-0.4738271	0.026
0.7	$(\pi, 0)$ spiral	-0.49363(1)	-0.5103811	0.033
0.8	$(\pi, 0)$ spiral	-0.52908(1)	-0.5500986	0.038
0.9	$(\pi, 0)$ spiral	-0.56719(1)	-0.5919934	0.042
1.0	$(\pi, 0)$ spiral	-0.60742(1)	-0.6355307	0.044

TABLE IV. Comparison between the exact ground-state energies and the energies of the best Jastrow wave function on the $4 \times 4 \times 2$ cluster for the Heisenberg model.

the Heisenberg model, the trend is similar to the previous one, even though the actual accuracy is always lower than in the XY model. The best variational energies are obtained in the unfrustrated regime (about 1.2%). Again, the worst accuracy appears for $J_2/J_1 = 0.3$, where a non-magnetic phase is expected to occur in the thermodynamic limit. Then a substantial improvement is obtained for $J_2/J_1 = 0.4$, but from there, the accuracy monotonically deteriorates on increasing the frustrating ratio, still remaining below 5% up to $J_2/J_1 = 1$. Note that, for larger clusters, the Néel state has a lower energy than the collinear state for $J_2/J_1 = 0.3$, while the collinear state has a lower energy than the $(\pi, 0)$ -spiral for $J_2/J_1 \gtrsim 0.7$.

-
- [1] *Introduction to Frustrated Magnetism*, edited by C. Lacroix, P. Mendels, and F. Mila, Springer Series in Solid-State Sciences Vol. 164 (Springer, Berlin, 2011).
- [2] H.-C. Jiang, H. Yao, and L. Balents, *Phys. Rev. B* **86**, 024424 (2012).
- [3] W.-J.Hu, F. Becca, A. Parola, and S. Sorella, *Phys. Rev. B* **88**, 060402 (2013).
- [4] S. Yan, D. Huse, and S. White, *Science* **332**, 1173 (2011).
- [5] Y. Iqbal, F. Becca, S. Sorella, and D. Poilblanc, *Phys. Rev. B* **87**, 060405 (2013).
- [6] T. Holstein and H. Primakoff, *Phys. Rev.* **58**, 1908 (1940).
- [7] P. Chandra, P. Coleman, and A.I. Larkin, *Phys. Rev. Lett.* **64**, 88 (1990).
- [8] M. Takahashi, *Phys. Rev. B* **40**, 2494 (1989).
- [9] E. Manousakis, *Rev. Mod. Phys.* **63**, 1 (1991).
- [10] S. Liang, B. Doucot, and P.W. Anderson, *Phys. Rev. Lett.* **61**, 365 (1988).
- [11] D.A. Huse and V. Elser, *Phys. Rev. Lett.* **60**, 2531 (1988).
- [12] M. Boninsegni, *Phys. Lett. A* **216**, 313 (1996).
- [13] F. Franjic and S. Sorella, *Prog. Theor. Phys.* **97**, 399 (1997).
- [14] A. Mulder, R. Ganesh, L. Capriotti, and A. Paramekanti, *Phys. Rev. B* **81**, 214419 (2010).
- [15] B.K. Clark, D.A. Abanin, and S.L. Sondhi, *Phys. Rev. Lett.* **107**, 087204 (2011).
- [16] A.F. Albuquerque, D. Schwandt, B. Hetenyi, S. Capponi, M. Mambrini, and A.M. Lauchli, *Phys. Rev. B* **84**, 024406 (2011).
- [17] D.J.J. Farnell, R.F. Bishop, P.H.Y. Li, J. Richter, and C.E. Campbell, *Phys. Rev. B* **84**, 012403 (2011).
- [18] J. Reuther, D.A. Abanin, and R. Thomale, *Phys. Rev. B* **84**, 014417 (2011).
- [19] J. Oitmaa and R.R.P. Singh, *Phys. Rev. B* **84**, 094424 (2011).
- [20] F. Mezzacapo and M. Boninsegni, *Phys. Rev. B* **85**, 060402 (2012).
- [21] R. Ganesh, J. van den Brink, and S. Nishimoto, *Phys. Rev. Lett.* **110**, 127203 (2013).
- [22] Z. Zhu, D.A. Huse, and S.R. White, *Phys. Rev. Lett.* **110**, 127205 (2013).
- [23] S.-S. Gong, D.N. Sheng, O.I. Motrunich, and M.P.A. Fisher, *Phys. Rev. B* **88**, 165138 (2013).
- [24] E. Rastelli, A. Tassi, and L. Reatto, *Physica B* **97**, 1 (1979).
- [25] J.B. Fouet, P. Sindzingre, and C. Lhuillier, *Eur. Phys. J. B* **20**, 241 (2001).
- [26] C.N. Varney, K. Sun, V. Galitski, and M. Rigol, *Phys.*

- Rev. Lett. **107**, 077201 (2011).
- [27] C.N. Varney, K. Sun, V. Galitski, and M. Rigol, New J. Phys. **14**, 115028 (2012).
- [28] J. Carrasquilla, A. Di Ciolo, F. Becca, V. Galitski, and M. Rigol, Phys. Rev. B **88**, 241109(R) (2013).
- [29] Z. Zhu, D.A. Huse, and S.R. White, Phys. Rev. Lett. **111**, 257201 (2013).
- [30] S. Sorella, Phys. Rev. B **71**, 241103 (2005).
- [31] S. Yunoki and S. Sorella, Phys. Rev. B **74**, 014408 (2006).
- [32] D.S. Fisher, Phys. Rev. B **39**, 11783 (1989).
- [33] H. Neuberger and T. Ziman, Phys. Rev. B **39**, 2608 (1989).
- [34] A.W. Sandvik, Phys. Rev. B **56**, 11678 (1997).